A new neutron depth profiling spectrometer at the JCNS for a focused neutron beam

E. Vezhlev, A. Ioffe, S. Mattauch, S. Staringer, V. Ossovyi, Ch. Felder, E. Hüger, J. Vacik, I. Tomandl, V. Hnatowicz, C. Chen, P.H.L. Notten & Th. Brückel

Published online: 30 Mar 2020.

Submit your article to this journal ⧉

View related articles ⧉

View Crossmark data ⧉

Taylor & Francis
Taylor & Francis Group

A new neutron depth profiling spectrometer at the JCNS for a focused neutron beam

E. Vezhlev[a], A. Ioffe[a], S. Mattauch[a], S. Staringer[a], V. Ossovyi[a], Ch. Felder[a], E. Hüger[b], J. Vacik[c], I. Tomandl[c], V. Hnatowicz[c], C. Chen[d,e], P.H.L. Notten[d,e,f] and Th. Brückel[g]

[a] Jülich Centre for Neutron Science (JCNS-4) at MLZ, Forschungszentrum Jülich GmbH, Garching, Germany; [b] Institute of Metallurgy Thermochemistry and Microkinetics, Technical University of Clausthal, Clausthal-Zellerfeld, Germany; [c] Nuclear Physics Institute, Academy of Sciences of the Czech Republic, Czech Republic Research Center Rez, Rez, Czech Republic; [d] Eindhoven University of Technology, MB Eindhoven, The Netherlands; [e] Institute of Energy and Climate Research, Fundamental Electrochemistry (IEK-9) Forschungszentrum Jülich GmbH, Jülich, Germany; [f] University of Technology Sydney, Ultimo, NSW , Australia; [g] Jülich Centre for Neutron Science (JCNS-2), Peter Grünberg Institut (PGI-4) Forschungszentrum Jülich GmbH, Jülich, Germany

ABSTRACT

A new neutron depth profiling (NDP) spectrometer has been designed and built for the use at a high intensity focused cold neutron beam of the reflectometer MARIA at the Heinz Maier-Leibnitz Zentrum (MLZ, Germany). The extremely high neutron flux at the sample position of MARIA joined with the multiple charged particle detectors allows less than 10 s sampling rate and paves the way to study the kinetics of Li ions in thin-film microbatteries. The performance of the spectrometer with standard calibration samples and *LiNbO₃* amorphous thin films is presented; possibilities to *operando* study the *Li* distribution inside thin-film rechargeable lithium batteries are discussed.

1. Introduction

Neutron depth profiling is a non-destructive analytical tool to study near-surface distributions of some light isotopes with high neutron capture cross-sections (^3He, ^6Li, ^{10}B, ^{14}N, ^{22}Na and few more) in solid materials. The neutron-absorption results in nuclei decay with the emission of a charged particle (α-particle, proton or triton) and a recoiling nucleus with well-known initial energies E_0. These particles are emitted isotropically and before escaping a sample surface, each particle looses a certain amount of energy $\Delta E = E_0 - E(x)$ mainly because of the interactions with the atomic electrons of the host material. The amount of energy losses ΔE defines the depth x at which the particle was created:

$$x = \int_{E(x)}^{E_0} \frac{dE}{dE/dx},$$

(1)

CONTACT E. Vezhlev ✉ e.vezhlev@fz-juelich.de

where dE/dx represents the stopping power of the host material for a charged particle. A raw spectrum already depicts the concentration profile of the analyzed element. The spectrum can be unfolded taking the instrument resolution function and possible uncertainties into account ([1]). By using measurements with a calibrated sample, the concentration depth profile can be derived in absolute units.

The NDP technique was first reported by J. Ziegler, G. W. Cole and J. E. E. Baglin in 1972 as a non-destructive tool to study ^{10}B impurities inside silicon substrates ([1]). Around the same time and independently similar experimental approach was used by J. P. Biersack and D. Fink ([2]). Later on, the technique was further advanced and a number of NDP instruments appeared around the world (e.g. ([3–5])). In the 1990s, the first up to our knowledge NDP facility utilizing a cold neutron beam from a cold source was built at NIST (Gaithersburg, Maryland, USA) ([6]). While a cold neutron beam has lower mean energy of the spectrum, it results in stronger neutron absorption, thus, improving the sensitivity (minimum observable concentrations of the analyzed elements) and decreasing the measurement time.

A further step, utilizing a cold neutron beam transported along a neutron guide, was first realized by D.Fink and coworkers at HMI, Berlin, Germany ([2]). Guided neutron beamlines offer much better background conditions in comparison with the beamlines located in the close vicinity of a research reactor and still deliver a high cold neutron flux. NDP technique advances here a lot in sensitivity, in ability to measure fast, in exploring thicker samples and in detection efficiency of low energy reaction products. During the last decade, NDP facilities utilizing guided cold neutron beams have been built at two new research reactor facilities – at HANARO (KAERI, Republic of Korea) ([7]) and at CMRR (INPC, CAEP, China) ([8]).

For more details about the NDP technique, its history and applications, we refer the reader to ([2]). Almost all NDP references up to the present compiled by R.G. Downing can be found at (https://sites.google.com/site/nistndp/home).

Recently, a demanding studies of lithium-ion batteries (LIB) created a new interest in the NDP technique because of its sensitivity to isotope ^6Li. NDP offers here a number of advantages. As NDP can be considered non-destructive, *Li* distribution inside a battery cell can be studied *operando* during battery charging and discharging for many cycles. After the data unfolding procedure, Li concentration is obtained quantitatively, which is hardly possible for Li by other methods. The natural limitations of the NDP technique, such as a limited range of charged particles in solids and sensitivity to sample roughness and homogeneity, limits the application mainly to thin solid-state planar batteries. Only in this case, an Li profile through the entire battery cell can be derived with high resolution by analysis of α-particle signal. Examples of NDP being applied to *operando* study solid-state thin-film LIB can be found in ([9], [10]). The moderate neutron flux and single charged particle detector available at the NDP facility ([9], [10]) made 10 min measurement time for a single NDP spectrum possible. To be able to get a single spectrum faster, we proposed to perform NDP experiments on a focused cold neutron beam with multiple charged particle detectors ([11]). Following this idea, we designed and built a dedicated NDP spectrometer at the JCNS for the use at high-intense vertically focused cold neutron beam of the reflectometer MARIA ([12]). In this paper, we are going to report on spectrometer specifications and performance with standard as well as real samples.
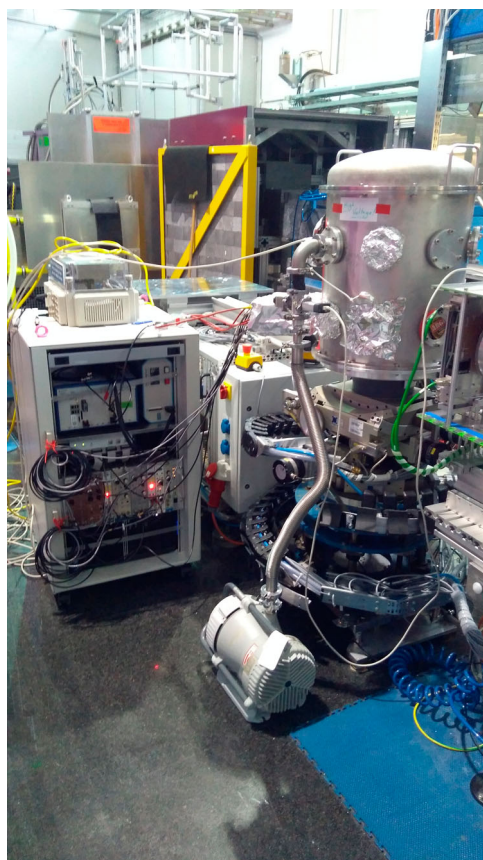
2. JCNS NDP spectrometer

2.1. Neutron beamlines

The reflectometer MARIA is facing a cold neutron guide NL5 that is fed by the cold neutron source of research reactor FRM II ([13]). The last part of the instrument neutron guiding system is a vertically focusing elliptic guide that delivers the neutron beam from a 10% velocity selector to the sample position. The maximum flux of $2.5 * 10^8$ n/cm^2/s is achieved for the uncollimated beam with 5 Å neutrons (thermal equivalent flux of $0.7 * 10^9$ n/cm^2/s). The beam size at the sample position can be as large as 5×2 cm^2 (width x height). The beam can be shaped horizontally by the two pairs of slits before and after a focusing guide that allows precise collimation of the neutron beam in respect to the sample dimensions, allowing us to avoid the over illumination of the sample and, thus, minimizing the background that could be created after neutron-induced activation of the chamber and its internal parts. Neutron beam monitors of MARIA can be used to calibrate each NDP measurement in respect to reactor / cold source performance. The NDP chamber is placed with a stationary holder on the MARIA sample table. To align a sample, the chamber is used in transmission mode with a position-sensitive detector of MARIA. Horizontal and vertical scanning is defining precisely the position of an absorbing sample in the beam. During NDP measurements, the beamstop made of ^6Li-polymer shielding is placed between the chamber and detector arm of MARIA. The schematic CAD drawing of the setup is shown in Figure 1.

For conventional (without fast kinetics) or preliminary measurements, the spectrometer keeps the versatility to operate at the medium flux test reflectometer TREFF available in the neutron guide hall of FRM II, MLZ ([14]). TREFF is a high resolution reflectometer where beam is cut from the lower part of a neutron guide NL5 with a double PG-monochromator (set to 4.74 Å primary wavelength). The maximum flux at the sample position including higher orders of reflection from a monochromator reaches 10^7 n/cm^2/s (width x height) for uncollimated beam. Two parallel monochromators create a neutron beam of the size of appr. 3×10 m^2 that can be further shaped by two pairs of slits along the reflectometer collimation. The procedure of alignment and measurements is similar to described above for MARIA. The spectrometer installed at TREFF is shown in Figure 2.
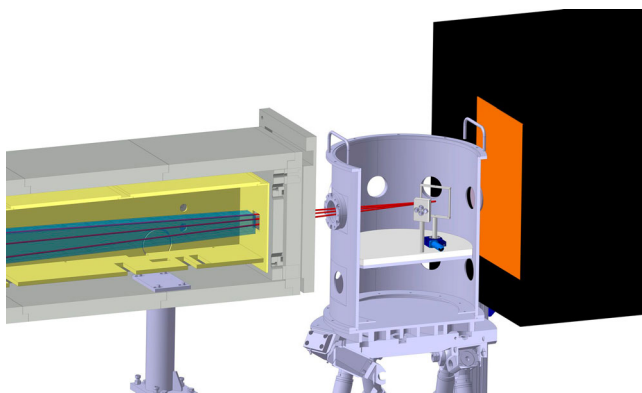
Figure 1. CAD drawing of the JCNS NDP chamber installed on the sample table of reflectometer MARIA. Cut-view.

Figure 2. NDP spectrometer installed at the sample position of the reflectometer TREFF.

2.2. Sample chamber

The NDP vacuum sample chamber is made from stainless steel and is equipped with 16 vacuum flanges. Four flanges are used to neutron beam entrance/exit at different heights depending on the beamline (MARIA or TREFF). The flanges have an approximately 0.1 mm thick aluminum alloy windows with 70 mm opening for a neutron beam. Rest of the ports are used for detector electronics connection, motorized stages, vacuum pump connection and reserved for future application. The chamber has a cylindrical shape, the inner dimensions are $\oslash 600 \times 500$ mm – to have enough space for a multiple detector system, shielding and to be able to house sample environment if required. The interior of the chamber can be accessed via the top spherical stainless steel cap. The desired vacuum level of less than 10^{-2} mbar is achieved in less than 5 min.

The detector holder(s) and the sample holder are placed inside the chamber on a 20 mm thick PTFE plate, which is supported by 10 mm thick aluminum plate (see Figure 3). The plates can be fixed at two different heights, providing flexibility for different beamlines. Holders for the sample and detector(s) are also made of PTFE to minimize possible background caused by neutron-induced activation and to keep the detectors electrically isolated from the chamber. Sample holders have thin PTFE wires for fixing a sample. Despite
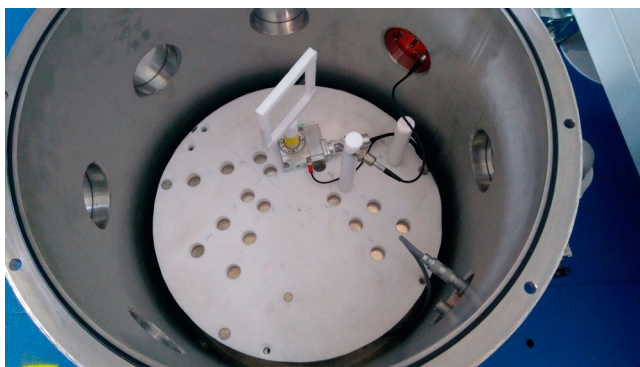
Figure 3. The interior of the NDP sample chamber with standard sample holder and single detector. Radiation shielding is removed for visibility.

the extremely thin aluminum entrance window and PTFE interior, gamma background is still produced and additional lead shielding of charged particle detectors inside is required (not shown in Figure 3 for better visibility).

The spectrometer is at present equipped with up to 4 PIPS (© Canberra GmbH) charged particle detectors, while more detectors are planned for the near future. The active area of the standard detector is 50 mm². The detector(s) can be placed at different angles both by rotating a sample with a rotation stage and by placing mechanically detector(s) at different angles. The distance between sample and detector can be changed between 35 and 150 mm, thus giving an opportunity to decrease/increase the solid acceptance angle for a single standard detector up to eight times. Alternatively, larger (150 mm²) or smaller (25 mm²) detectors can be used. All these options give a versatility for tuning the resolution versus counting rate in each particular measurement.
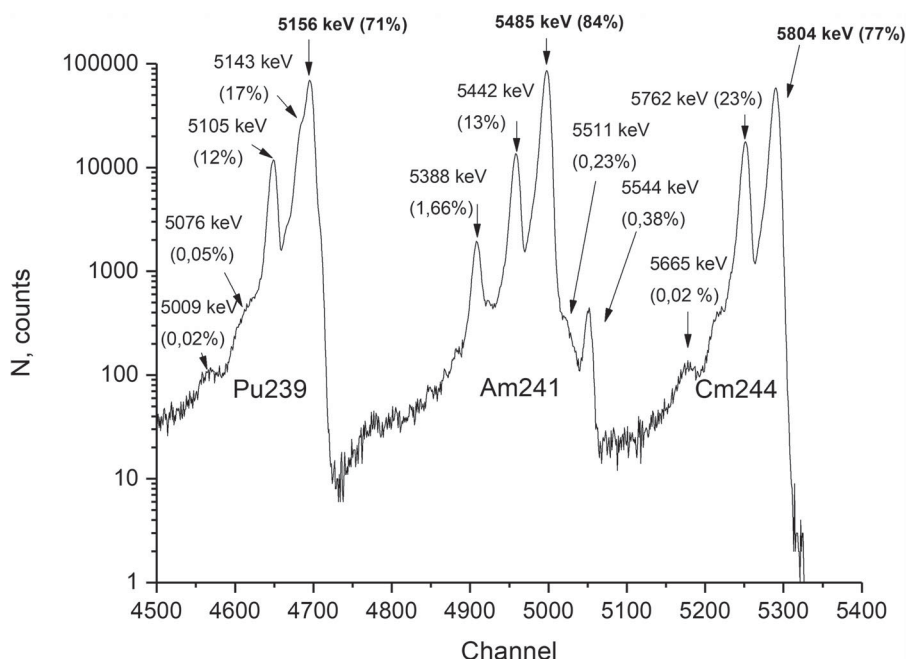
2.3. Electronics

The schematic view of the readout chain, as well as the schematic representation of the pulse height analysis procedure, are shown in Figure 4. The signals from charged particle detectors are further processed in the charge-integrating preamplifier (CSP), main spectroscopy shaping amplifier with further fast analog to digital converter (ADC) to digitize the pulses and multi-channel analyzer (MCA) to save the spectra and forward it into the PC. MCA range can be preset to different values depending on the counting rate and resolution requirements. By default, the range is 8192 number of energy channels. The preamplifiers
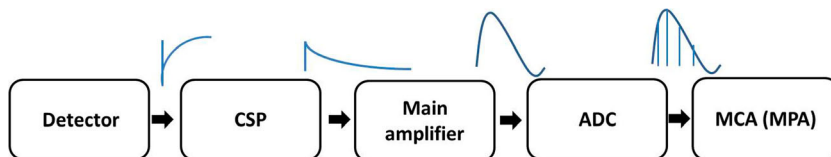
Figure 4. A block diagram of the detector signal readout chain of JCNS NDP spectrometer.

Figure 5. Spectrum collected from a 3 kBq mixed α-particle source (^{239} Pu, ^{241} Am, ^{244} Cm) with 30 mm sample to detector distance.

are fixed directly at one of the chamber ports while all further electronics is housed in a stand-alone rack (see Figure 2).

We have tested the detector readout chain with 3kBq mixed α-particle source (^{241} Am, ^{239} Pu, ^{244} Cm). The spectrum is shown in Figure 5. If we calculate the calibration parameters between the most pronounced peaks of Cm (5804 keV) and Pu (5156 keV), it results in $\approx$ 1.1 keV per 1 MCA channel for a corresponding energy range, giving the energy resolution of $\Delta E \approx 11$ keV in this energy range for the detection of α-particles. The obtained energy resolution of 11 keV coincides with the value declared by the manufacturer of detectors.

3. Performance of the new NDP spectrometer with standard NDP samples and ^{6}LiNbO$_3$ thin films.

To get the spectrometer characteristics during neutron measurements, NDP standard samples and specially deposited ^{6}LiNbO$_3$ thin films have been measured at MARIA. Energy resolution parameters were obtained from the measurement of standard reference material sample SRM93a (NIST, USA). The sample consists of a 6 mm thick, 32 mm wide in diameter piece of borosilicate glass (with 12.5%B$_2$O$_3$ content) and can be used to perform energy-channel calibration of NDP detecting system (7). The signal created after neutron capture should have a uniform distribution with a steep edge for highest energies (particles from a surface) of 1472 and 1776 keV (see Figure 6). Below the channel 480, the contribution from γ-signal coming from the sample itself (i.e. 480 keV γ-rays produced after neutron capture in ^{10}B) appears. As the reaction cross-section for the first reaction channel is considerably larger (counting statistics is correspondingly proportional) – the energy edge for
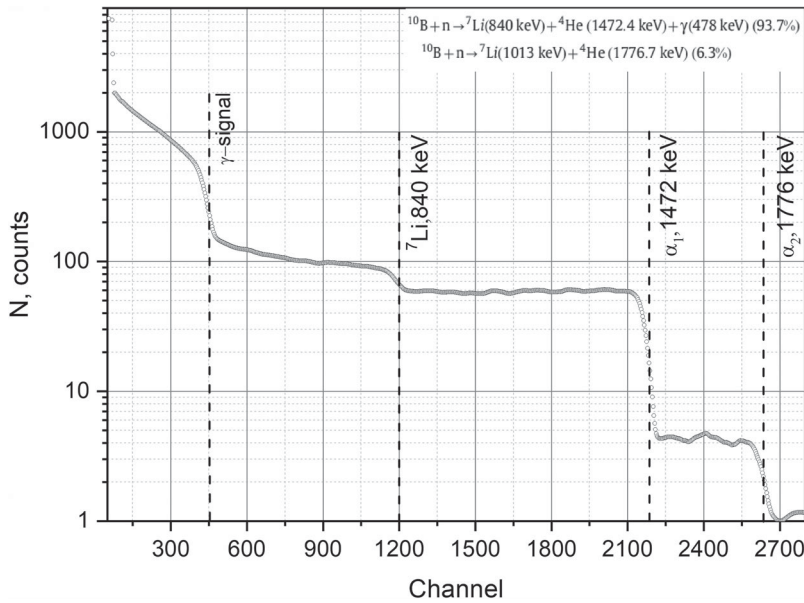
Figure 6. Spectrum collected from SRM–93a borosilicate glass. Highest energies (particles from the sample surface) are marked with dashed lines.

1472 keV is used to determine the resolution parameters. The 90 min measurement has been performed with the sample to detector distance of 100 mm.

The smoothed first derivative of the energy edge for 1472 keV gives a bell shape curve with FWHM of 11 keV (see Figure 7), that can be considered as the spectrometer energy resolution for α-particles produced after $^{10}B(n,^4He)^7Li$ reaction.

The theoretically achievable depth resolution in NDP analysis can be estimated according to (15):

$$\Delta x = \Delta E \cdot \frac{\cos\theta}{dE/dx},$$

(2)

where θ is the angle between the detector and sample normal, dE/dx represents stopping power of host material, ΔE – uncertainty in measured energy loss. For calculating ΔE, we have taken the following parameters into account (15): energy resolution, uncertainty of θ within the solid acceptance angle of the detector, effects from energy struggling and nuclear scattering. We have estimated the achievable depth resolution for a typical thin-film LIB component $LiCoO_2$ electrode film as a function of the angle θ (see Figure 8). The resolution for standard geometry (detector surface is perpendicular to the sample surface normal) exceeds 35 nm, while resolution for glancing angles geometry ($74° \leq \theta \leq 84.5°$) is less than 10 nm (the estimate is given with the assumption of 100 nm thin sample and 3.5 g/cm^3 density, the stopping power was calculated with SRIM software[1] and was taken to be constant for simplicity).

For unfolding of the measured raw data, the determination of the detector energy response function is required. Any measured spectra $S(E)$ is a concentration profile of an analyzed isotope $C(x)$ convoluted with the detector response function $f_{det}(E,x)$ that
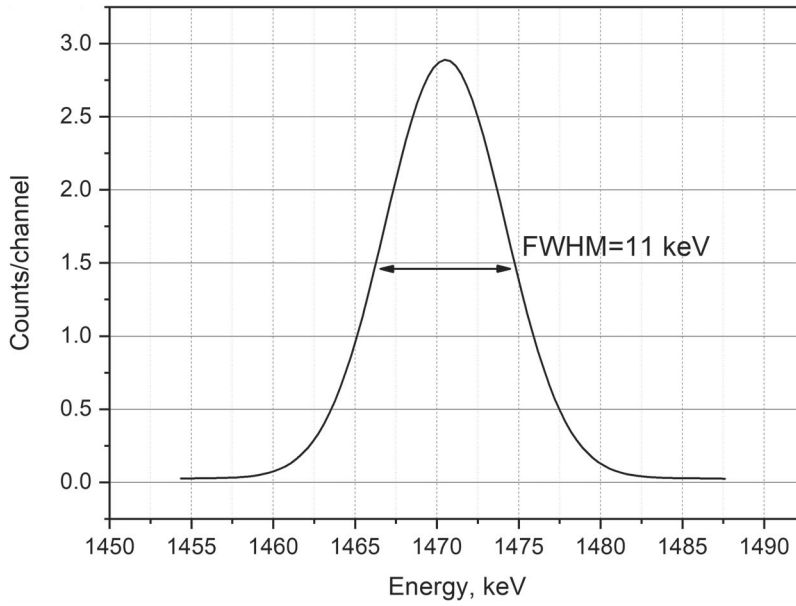
Figure 7. Inverted first derivative of the energy edge 1472 keV. Represents energy resolution of the NDP detectors system.
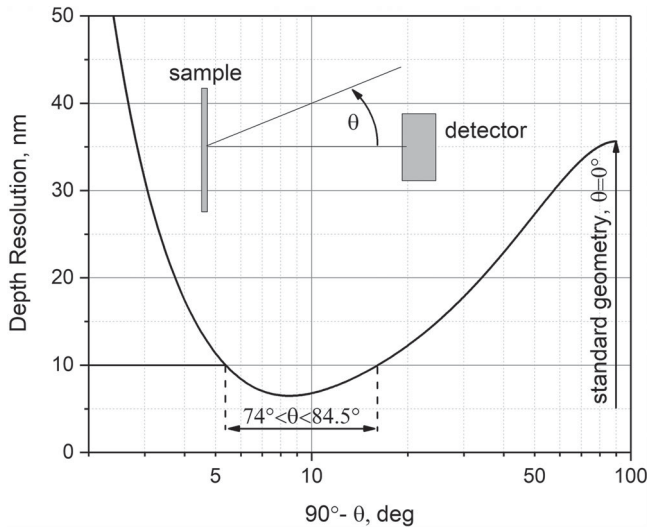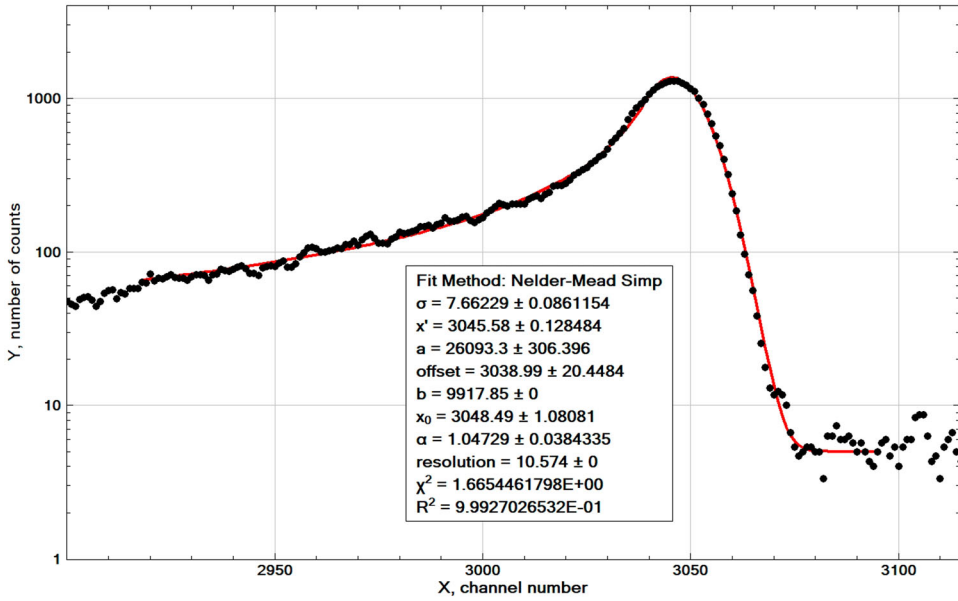

Figure 8. Achievable depth resolution for the 100 nm $LiCoO_2$ thin film.

includes possible uncertainties in measured energy and background (*16–19*):

$$S(E) = \int C(x) \cdot f_{det}(E, x) \, dx,$$ (3)

the response function $f_{det}(E, x)$ here gives a probability of a particle emitted from depth x being detected with energy E. The response function can be simulated (*17–19*) or it can

Figure 9. α-signal collected from 15 nm thick $^6\text{LiNbO}_3$ thin film (circles) and a fit (solid line).

be derived for particular isotope and sample from the measurement. To derive one for α-particles[2] emitted after $^6\text{Li}(n,^3\text{H})^4\text{He}$ reaction, we have been using 15 nm thick $^6\text{LiNbO}_3$ (95% ^6Li) amorphous thin film deposited on a silicon substrate. For a standard geometry, the layer of 15 nm is less then theoretical resolution with α-particle for $^6\text{LiNbO}_3$ thin film (which is $\approx$ 30 nm for 100 nm film with 4.65 g/cm^3 density), so we assume that 15 nm thin film acts as a 'single' layer and the measured spectrum represents a pure detector response. The measured α-signal and the fit are shown in Figure 9. As a fitting function, we used a Gaussian function for the main peak and power law on the left tail of the peak by the analogy with (20):

$$y = \begin{cases} \dfrac{a}{\sigma\sqrt{2\pi}} \cdot \exp\left(-\dfrac{1}{2} \cdot \left(\dfrac{x - x_0}{\sigma}\right)^2\right), & x \geq x' \\ \dfrac{b}{(x_0 - x)^{\alpha}}, & x \leq x' \end{cases} \tag{4}$$

where x' is set manually to the channel number 3038. The left tail is produced mostly due to incomplete collection of charge generated by α-particles in the detector. The peak form which is nearly Gaussian with $FWHM = 11$ keV (in accord with the spectrometer resolution mentioned above) represents the response function for particles emitted from a 'single' layer or the sample surface. For the particles emitted from the sample interior, the width of the response function will increase due to contributions from statistical fluctuations in particle energy loss (multiple scattering, energy straggling, etc.). As well the response function can be also affected by the geometrical arrangement of an experiment (*e.g.* for glancing angle geometry).
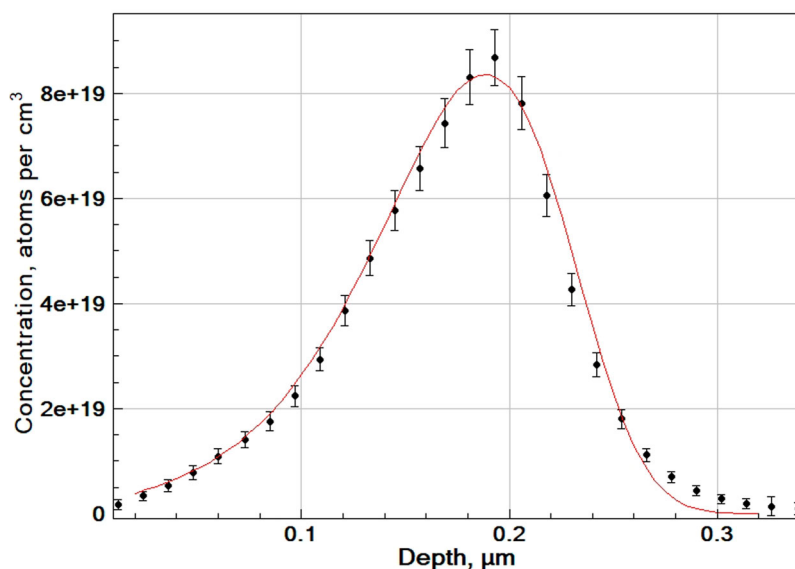
Figure 10. Unfolded NDP spectrum of SRM–2137 collected on MARIA in roughly 14h. Solid line – certified values, dots – as measured.

Consequently, NDP calibration standard SRM2137 (NIST) has been measured (Figure 10). The sample consists of boron implanted into a silicon wafer. The Boron depth distribution is certified by NIST after performing several secondary ion mass spectrometry (SIMS) measurements. The unfolded depth profile after NDP measurement and comparison to the certified Boron distribution are shown in Figure 10. The unfolding procedure has been
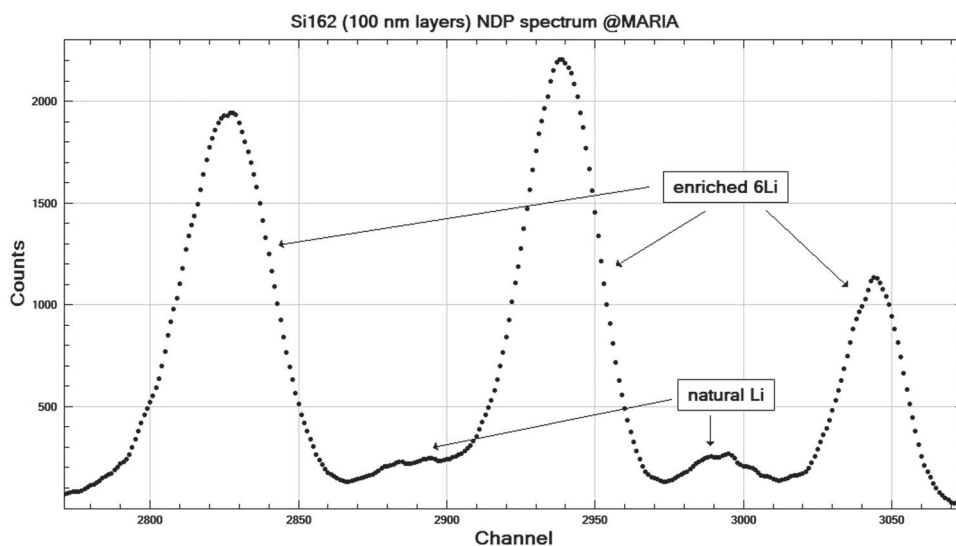
Figure 11. α-peak region of the smoothed spectrum collected for multilayer thin-film sample $^6\text{LiNbO}_3/\text{Si}/^{nat}\text{LiNbO}_3$.

performed using the software developed in (*16*, *21*). Small deviations on the right shoulder are caused by the above-mentioned asymmetry in detector response function while the available software operates only with symmetric Gaussian response.

To improve the statistics during the NDP measurements, deposition of the samples with enrichment of neutron-absorbing isotopes should be considered. For example, for ^{6}Li-enriched samples a gain factor of up to 13 in comparison with natural ^{6}Li-abundance samples (7,5%) can correspondingly reduce the minimum time required to get a desired spectrum. To prove this idea, a thin film $LiNbO_3$ sample, having ^{6}Li-enriched layers, has been measured. The structure of the sample is as follows: three $^6LiNbO_3$ layers, two (^{nat}Li)NbO_3 layers and 4 Si spacer layers in between, The ^{6}Li isotope fraction of the $^6LiNbO_3$ and $^{nat}LiNbO_3$ layers is 0.95 and 0.07, respectively. The thicknesses of the $LiNbO_3$ layers and Si spacer layers are 45 nm and 95 nm, respectively. All $LiNbO_3$ layers have an amorphous structure. The measured spectrum is shown in Figure 11. As expected, ^{6}Li-enriched layers are giving 13 times stronger signal with respect to absorbing isotope abundance. For *operando* studies of thin-film batteries, the deposition of samples with ^{6}Li-enriched layers is certainly of advantage.
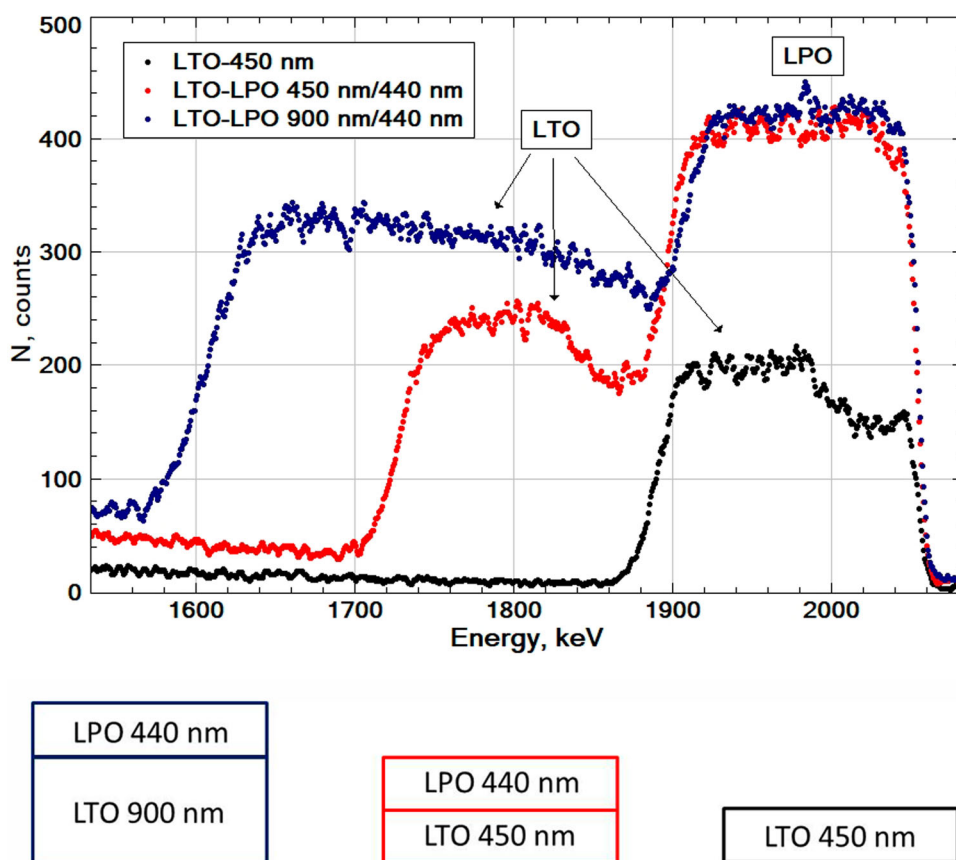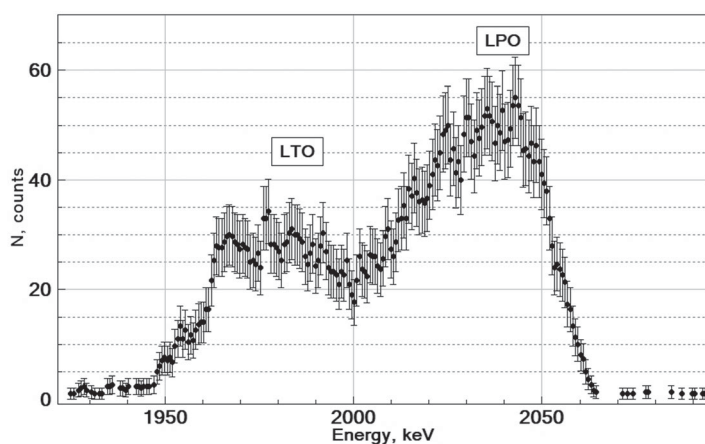

Figure 12. Smoothed spectra collected on MARIA in 90 minutes for thin films – single film $Li_4Ti_5O_{12}$ (LTO) and double layer films $Li_4Ti_5O_{12}/Li_3PO_4$ (LTO–LPO).

4. Test measurements with lithium thin-film batteries.

The next step in exploring the capabilities of the new spectrometer were the measurements of thin-film Li-ion battery samples in their as-deposited state. Thin-film half cell battery samples of different thicknesses – comprising single electrode film $Li_4Ti_5O_{12}(450\,nm)$ and electrode/electrolyte films $Li_4Ti_5O_{12}(190\,nm, 450\,nm, 900\,nm) - Li_3PO_4(180\,nm, 440\,nm)$ were deposited on silicon substrates by metal-organic chemical vapor deposition method (MOCVD). Spectra collected for 90 min from $Li_4Ti_5O_{12}(450\,nm)$
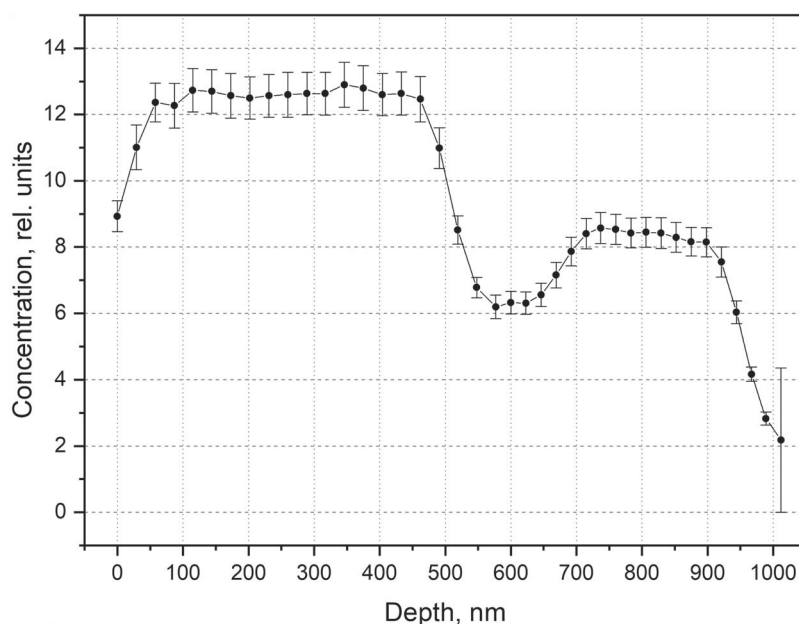
Figure 13. Unfolded Li depth profile (in relative units) of $Li_4Ti_5O_{12}/Li_3PO_4$ film.

Figure 14. Smoothed spectra collected on MARIA for $Li_4Ti_5O_{12}(190\,nm) - Li_3PO_4(180\,nm)$ sample (LTO–LPO).

and $Li_4Ti_5O_{12}(450\,nm, 900\,nm) - Li_3PO_4(440\,nm)$ films are shown in Figure 12. The example of unfolded spectrum for the thickest sample is shown in Figure 13. All samples in this section were deposited with the natural abundance (not exceeding 7.5%) of neutron-absorbing isotope ^6Li.

The counting time that will be required for reliable measurements of a battery-type sample can be estimated using the result of 10 min measurements of thin-film $Li_4Ti_5O_{12}(190\,nm) - Li_3PO_4(180\,nm)$ (see Figure 14). Despite of short measurement time, the statistical errors are still sufficiently small and do not mask the observed features – the difference in Li concentration between electrode $Li_4Ti_5O_{12}$ and electrolyte Li_3PO_4. The use of fully ^6Li-enriched samples and 8 detectors of charged particles will result in 13 and 8 times increase in the number of collected charged particles, respectively. Indeed, in such case, the same counting statistics will be achieved within the data collection time of less than 10 s. Such an extremely fast *operando* NDP studies of LIB during charging and discharging have been never realized before and should give a clearer picture of the battery chemistry evolution in time.

5. Conclusions

A new neutron depth profiling spectrometer has been designed and made operational at the focused cold neutron beam of the JCNS reflectometer MARIA. The spectrometer has been tested and characterized with standard NDP samples and different amorphous $(^{nat}Li,^6Li)NbO_3$ thin films. The measurements of thin-film LIB samples in as-deposited state provided the information on the achievable rate for *operando* studies – single meaningful NDP spectrum can be obtained for a ^6Li-enriched thin-film LIB in less than 10 s. Further steps to improve the spectrometer performance, such as using a 2-D focused neutron beam, increasing the number of charged particle detectors and further reduction of the background, are planned for the near future.

Notes

1. http://www.srim.org.
2. In this paper, we focus only on α-particle part of spectra for $^6Li(n,^3H)^4He$ products, as signal from α-particles provides significantly higher depth resolution than ^3H-signal.

Disclosure statement

No potential conflict of interest was reported by the authors.

Funding

References

(1) Ziegler, J.F.; Cole, G.W.; Baglin, J.E.E. *J. Appl. Phys.* **1972**, *43*, 3809–3815.
(2) Fink, D. *Neutron Depth Profiling*, HMI-B 539, HMI Berlin, Germany, 1996.
(3) Müller, K.; Henkelmann, R.; Boroffka, H. *Nucl. Inst. Methods* **1975**, *129*, 557.

(4) Downing, R.G.; Fleming, R.F.; Langland, J.K.; Vincent, D.H. *Nucl. Inst. Methods Phys. Res.* **1983**, *218*, 47–51.

(5) Cervena, J.; Hnatowicz, V.; Hoffman, J.; Kosina, Z.; Kvitek, J.; Onheiser, P. *Nucl. Inst. Methods* **1981**, *188*, 185–189.

(6) Downing, R.G.; Lamaze, G.P.; Langland, J.K.; Hwang, S.T. *J. Res. Natl. Inst. Stand. Technol*. **1993**, *98*, 109–126.

(7) Park, B.G.; Sun, G.M.; Choi, H.D. *Nucl. Inst. Methods Phys. Res. A* **2014**, *752*, 20–26.

(8) Li, R.-D.; Yang, X.; Wang, G.-B.; Dou, H.-F.; Qian, D.-Z.; Wang, S.-Y. *Nucl. Inst. Methods Phys. Res. A* **2015**, *788*, 1–4.

(9) Oudenhoven, J.F.M.; Labohm, F.; Mulder, M.; Niessen, R.A.H.; Mulder, F.M.; Notten, P.H.L. *Adv. Mater*. **2011**, *23*, 4103–4106.

(10) Chen, C.; Oudenhoven, J.F.M.; Danilov, D.L.; Vezhlev, E.; Gao, L.; Li, N.; Mulder, F.M.; Eichel, R.-A.; Notten, P.H.L. *Adv. Energy Mater*. **2018**, *8*, 1801430.

(11) Vezhlev, E. *Neutron Depth Profiling at the Focused Beam of MARIA*. Joint Annual Report 2015 of the MLZ and FRM II, 2017.

(12) Mattauch, S.; Koutsioubas, A.; Räcker, U.; Korolkov, D.; Fracassi, V.; Daemen, J.; Schmitz, R.; Bussmann, K.; Suxdorf, F.; Wagener, M.; Kämmerling, P.; Kleines, H.; Fleischhauer-Fuß, L.; Bednareck, M.; Ossoviy, V.; Nebel, A.; Stronciwilk, P.; Staringer, S.; Gödel, M.; Richter, A.; Kusche, H.; Kohnke, T.; Ioffe, A.; Babcock, E.; Salhi, Z.; Bruckel, T. *J. Appl. Crystallogr*. **May 29, 2018,** *51* (Pt 3), 646–654.

(13) FRM II – Heinz Maier-Leibnitz Zentrum: http://www.mlz-garching.de/.

(14) Heinz Maier-Leibnitz Zentrum. *J. Large-scale Res. Facil*. **2017**, *3*, A121.

(15) Biersack, J.P.; Fink, D.; Henkelmann, R.; Moller, K. *Nucl. Inst. Methods* **1978**, *149*, 93–97.

(16) Kotas, P.; Obrusnik, I.; Kvitek, J.; Hnatowicz, V. *J. Radioanal. Chem*. **1976**, *30*, 475–488.

(17) Coakley, K.J.; Downing, R.G.; Lamaze, G.P.; Hofsäss, H.C.; Biegel, J.; Ronning, C. *Nucl. Inst. Methods Phys. Res. A* **1995**, *366*, 137–144.

(18) Yang, X.; Downing, R.G.; Wang, G.B.; Qian, D.Z.; Liu, H.G.; Wang, K. *J. Radioanal. Nucl. Chem*. **2014**, *301*, 213–220.

(19) Dou, H.F.; Li, R.D.; Xu, J.Y.; Yuan, S.; Tang, F.P.; Yang, X. *Sci. China Technol. Sci.* **2014**, *57* (1), 35–38.

(20) Longoria, L.C.; Naboulsi, A.H.; Gray, P.W.; MacMahon, T.D. *Nucl. Inst. Methods Phys. Res*. **1990**, *A299*, 308–312.

(21) Hnatowicz, V.; Vacik, J.; Fink, D. *Rev. Sci. Ins*. **2010**, *81*, 073906.